Research Article | Vol. 25, No. 17 | 21 Aug 2017 | OPTICS EXPRESS 20194
Optics EXPRESS

Tailored intensity landscapes by tight focusing of singular vector beams

EILEEN OTTE,* KEMAL TEKCE, AND CORNELIA DENZ

Institute of Applied Physics, University of Muenster, Corrensstr. 2/4, 48149 Muenster, Germany
*eileen.otte@uni-muenster.de

Abstract: Vector beams are of major importance to tailor tightly focused fields by creating an additional *z*-polarization component. Till now, mainly focusing properties of fundamental vector beams have been investigated, whereas the knowledge of focused higher-order singular vector fields is still missing. We fill this gap by numerical analysis of these fields, applying their attractive characteristics as including a spatially adjustable amount of radial and azimuthal components. We demonstrate the realization of three-dimensional polarization structures whose total intensity resembles dark stars and bright flowers. Further, we tailor these focal intensity landscapes by modulating the order of incident vector fields. This in turn allows shaping the focus of a light field for specific applications as e.g. advanced microscopy.

Published by The Optical Society under the terms of the Creative Commons Attribution 4.0 License. Further distribution of this work must maintain attribution to the author(s) and the published article's title, journal citation, and DOI.

OCIS codes: (260.6042) Singular optics; (260.5430) Polarization; (050.4865) Optical vortices; (140.3300) Laser beam shaping.

References and links

1. H. Rubinsztein-Dunlop, A. Forbes, M. V. Berry, M. R. Dennis, D. L. Andrews, M. Mansuripur, C. Denz, C. Alpmann, P. Banzer, T. Bauer, E. Karimi, L. Marrucci, M. Padgett, M. Ritsch-Marte, N. M. Litchinitser, N. P. Bigelow, C. Rosales-Guzmán, A. Belmonte, J. P. Torres, T. W. Neely, M. Baker, R. Gordon, A. B. Stilgoe, J. Romero, A. G. White, R. Fickler, A. E. Willner, G. Xie, B. McMorran, and A. M. Weiner, "Roadmap on structured light," J. Opt. **19**, 013001 (2017).
2. E. J. Galvez, *Light Beams with Spatially Variable Polarization*, vol. 1 of *Photonics – Fundamentals of Photonics and Physics* (John Wiley & Sons, 2015)chap. 3, pp. 61–76.
3. J. F. Nye and M. V. Berry, "Dislocations in Wave Trains," Proceedings of the Royal Society of London A: Mathematical, Physical and Engineering Sciences **336**, 165–190 (1974).
4. M. Berry and C. Upstill, *Catastrophe Optics: Morphologies of Caustics and Their Diffraction Patterns* vol. 18 of *Progress in Optics* (Elsevier, 1980), chap. IV, pp. 257–346.
5. M. S. Soskin and M. V. Vasnetsov, *Singular Optics* vol. 42 of *Progress in Optics* (Elsevier, 2001), chap. 4, pp. 219–277.
6. M. R. Dennis, K. O'Holleran, and M. J. Padgett, *Singular Optics: Optical Vortices and Polarization Singularities* vol. 53 of *Progress in Optics* (Elsevier, 2009), chap. 5, pp. 293–363.
7. K. Dholakia and T. Čižmár, "Shaping the future of manipulation," Nature Photon. **5**, 335–342 (2011).
8. M. Taylor, M. Waleed, A. B. Stilgoe, H. Rubinsztein-Dunlop, and W. P. Bowen, "Enhanced optical trapping via structured scattering," Nature Photon. **9**, 669 (2015).
9. C. Alpmann, C. Schöler, and C. Denz, "Elegant Gaussian beams for enhanced optical manipulation," Appl. Phys. Lett. **106**, 241102 (2015).
10. J. J. Nivas, F. Cardano, Z. Song, A. Rubano, R. Fittipaldi, A. Vecchione, D. Paparo, L. Marrucci, R. Bruzzese, and S. Amoruso, "Surface structuring with polarization-singular femtosecond laser beams generated by a q-plate," Sci. Rep. **7**, 42142 (2017).
11. M. Meier, V. Romano, and T. Feurer, "Material processing with pulsed radially and azimuthally polarized laser radiation," Appl. Phys. A **86**, 329–334 (2007).
12. P. Rose, F. Diebel, M. Boguslawski, and C. Denz, "Airy beam induced optical routing," Appl. Phys. Lett. **102**, 101101 (2013).
13. S. W. Hell and J. Wichmann, "Breaking the diffraction resolution limit by stimulated emission: stimulated-emission-depletion fluorescence microscopy," Opt. Lett. **19**, 780–782 (1994).
14. L. Novotny, M. R. Beversluis, K. S. Youngworth, and T. G. Brown, "Longitudinal field modes probed by single molecules," Phys. Rev. Lett. **86**, 5251–5254 (2001).

#290807 https://doi.org/10.1364/OE.25.020194
Journal © 2017 Received 16 Mar 2017; revised 30 Apr 2017; accepted 1 May 2017; published 11 Aug 2017

Optics EXPRESS

15. K. Youngworth and T. Brown, "Focusing of high numerical aperture cylindrical-vector beams," Opt. Express **7**, 77–87 (2000).
16. R. Dorn, S. Quabis, and G. Leuchs, "Sharper focus for a radially polarized light beam," Phys. Rev. Lett. **91**, 233901 (2003).
17. R. W. Schoonover and T. D. Visser, "Polarization singularities of focused, radially polarized fields," Opt. Express **14**, 5733–5745 (2006).
18. W. Zhang, S. Liu, P. Li, X. Jiao, and J. Zhao, "Controlling the polarization singularities of the focused azimuthally polarized beams," Opt. Express **21**, 974–983 (2013).
19. I. Freund, "Cones, spirals, and Möbius strips, in elliptically polarized light," Opt. Commun. **249**, 7–22 (2005).
20. M. R. Dennis, "Fermionic out-of-plane structure of polarization singularities," Opt. Lett. **36**, 3765–3767 (2011).
21. T. Bauer, P. Banzer, E. Karimi, S. Orlov, A. Rubano, L. Marrucci, E. Santamato, R. W. Boyd, and G. Leuchs, "Observation of optical polarization Möbius stripes," Science textbf347, 964–966 (2015).
22. T. Bauer, M. Neugebauer, G. Leuchs, and P. Banzer, "Optical polarization möbius strips and points of purely transverse spin density," Phys. Rev. Lett. **117**, 013601 (2016).
23. Q. Zhan and J. R. Leger, "Microellipsometer with radial symmetry," Appl. Opt. **41**, 4630–4637 (2002).
24. W. Chen and Q. Zhan, "Three-dimensional focus shaping with cylindrical vector beams," Opt. Commun. **265**, 411 – 417 (2006).
25. N. Bokor and N. Davidson, "Generation of a hollow dark spherical spot by 4π focusing of a radially polarized Laguerre-Gaussian beam," Opt. Lett. **31**, 149–151 (2006).
26. Q. Zhan, "Cylindrical vector beams: from mathematical concepts to applications," Adv. Opt. Photon. **1**, 1–57 (2009).
27. H. Wang, L. Shi, B. Lukyanchuk, C. Sheppard, and C. T. Chong, "Creation of a needle of longitudinally polarized light in vacuum using binary optics," Nature Photon. **2**, 501–505 (2008).
28. F. Qin, K. Huang, J. Wu, J. Jiao, X. Luo, C. Qiu, and M. Hong, "Shaping a subwavelength needle with ultra-long focal length by focusing azimuthally polarized light," Sci. Rep. **5**, 9977 (2015).
29. E. Otte, C. Alpmann, and C. Denz, "Higher-order polarization singularitites in tailored vector beams," J. Opt. **18**, 074012 (2016).
30. I. Freund, "Polarization singularity indices in Gaussian laser beams," Opt. Commun. **201**, 251–270 (2002).
31. B. Richards and E. Wolf, "Electromagnetic diffraction in optical systems. II. Structure of the image field in an aplanatic system," in "Proceedings of the Royal Society of London A: Mathematical, Physical and Engineering Sciences" vol. 253 (The Royal Society, 1959), pp. 358–379.
32. B. Boruah and M. Neil, "Focal field computation of an arbitrarily polarized beam using fast fourier transforms," Opt. Commun. **282**, 4660–4667 (2009).
33. X. Pang, T. Visser, and E. Wolf, "Phase anomaly and phase singularities of the field in the focal region of high-numerical aperture systems," Opt. Commun.**284**, 5517–5522 (2011).

1. Introduction

Tailoring the structure of light has emerged as a powerful tool in fundamental research as well as in a wide range of applications [1]. Beyond amplitude and phase modulated light, in particular spatially structured polarization [2] lead to neoteric approaches for shaping light fields in the paraxial as well as the non-paraxial regime. On the one hand, these structured fields enables research on e.g. singular optics [3–6], i.e. the investigation of intensity, phase or polarization singularities. On the other hand, tailored light is of major significance for a myriad of advanced applications in optical trapping [7–9], material machining [10–12] or high-resolution microscopy [13, 14]. For the advancement of these applications it is of particular importance to understand tight focusing (numerical aperture NA $\geq$ 0.7) properties of tailored light in all its details.

Tightly focused polarization structures can exhibit longitudinal in addition to well known transverse electric field components [15, 16]. This property facilitates the creation of three-dimensional (3d) polarization structures including 3d polarization singularities [17, 18], topological structures [19–22], or shaping 3d intensity structures [15, 23–26]. For example, optical Möbius stripes were realized by focusing Poincaré beams embedding C-point singularities (singular points of circular polarization) [21, 22] or intensity structures as an optical bubble [24, 25] and needle [27, 28] were created by combining focusing properties of radially (RP) or azimuthally polarized (AP) beams with diffractive optical elements. RP and AP beams are widely used since RP parts are responsible for the generation of focal longitudinal components, whereas AP parts stay purely transverse [15]. The research to date has tended to

Optics EXPRESS

take advantage of this characteristic in mainly basic polarization strucutres as purely RP and AP vector beams or their superpositions rather than to exploit its full potential by using more complex beams.

In general, vector beams consist of only linear states of polarization with spatially varying orientation [2, 29]. Depending on the orientation of polarization, vector fields can embed V-point singularities, i.e. points of undefined polarization [29]. In named basic polarization structures, V-points are of lowest order, which means respective Poincaré-Hopf index is given by $\eta = \pm 1$ or Stokes field index $\sigma_{12} = 2\eta = \pm 2$ [29,30]. V-point singularities of index $|\sigma_{12}| > 2$ can be found in higher-order singular vector beams, whose polarization reveals the shape of a $|\sigma_{12} - 2|$-fold flowers and spider webs [29]. In contrast to previous investigations, these beams are not generable by superposition of purely RP and AP fields, but, however, include both, RP and AP components. The ratio of RP to AP parts, responsible for the strength of longitudinal and transverse focal field components, can be shaped spatially depending on the respective singularity index σ_{12}. Due to this feature, vectorial flowers and spider webs are very attractive to tailor focal field distributions. Nonetheless, tight focusing properties of these fields are scarcely known and its exploration is still in its infancy.

We demonstrate tight focusing characteristics of flower- and web-like, higher-order singular vector beam and, thereby, realize structured three-dimensional focal field distributions. These distributions result in sophisticated intensity landscapes resembling dark stars and bright flowers. Futhermore, we identify a relation between chosen singularity index σ_{12} of the input vectorial flower or web and the resulting focal intensity landscapes as well as the strength of transverse and longitudinal polarization components. Consequently, by modulating the index σ_{12} of incident flowers and webs, we are able to specifically shape the focal intensity structure for desired applications.

2. Higher-order singular vector beams

For the detection and analysis of V-point singularities in vector beams the complex Stokes field $\Sigma_{12} = S_1 + \mathrm{i}S_2 = A_{12}\exp(\mathrm{i}\Phi_{12})$ can be used [29, 30]. Here, $S_{1,2}$ represent normalized Stokes parameters (normalized Stokes vector $\vec{S} = (S_0, S_1, S_2, S_3)$, see [30]) of the investigated vector field, and A_{12} is the complex amplitude, Φ_{12} the phase of the Stokes field. If the phase Φ_{12} of a vector field reveals a vortex-like distribution, the central phase singularity depicts a V-point [29]. The characterizing index of this singular point is given by the counterclockwise change of phase around the singularity devided by 2π, i.e. $\sigma_{12} = \Delta\Phi_{12}/2\pi$. V-points and respective vector beams are of higher order if the corresponding singularity index is $|\sigma_{12}| > 2$ [29].

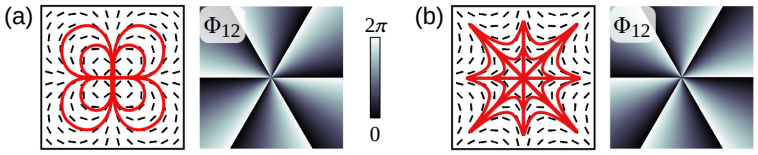

Fig. 1. Examples of higher-order singular vector beams with $\sigma_{12} = \pm 6$: Polarization distribution with red flow lines (left) and phase Φ_{12} of complex Stokes field (right) of a (a) $|\sigma_{12} - 2| = 4$-fold vectorial flower and (b) 8-fold spider web.

Higher-order singular vector beams reveal a specific shape in polarization according to the sign of included singularity's index [29, 30]: vector fields embedding a singularity of index $\sigma_{12} > 0$ or $\sigma_{12} < 0$ show the shape of a $|\sigma_{12} - 2|$-fold flower or spider web, respectively, as

Optics EXPRESS

described previously in [29]. In these cases, the electric field $\vec{E^i} = (E_x^i, E_y^i)^{\mathrm{T}}$ is defined by

$$\vec{E^i} = \left[\cos\left(\frac{\sigma_{12}}{2}\cdot\phi\right), \sin\left(\frac{\sigma_{12}}{2}\cdot\phi\right)\right]^{\mathrm{T}} \tag{1}$$

with $|\sigma_{12}|/2 \in \mathbf{N}$ and the azimuthal angle $\phi \in [0, 2\pi]$ in polar coordinates. An example of a vectorial flower and a web is illustrated in Fig. 1(a) and (b). Here, the left image shows the respective vector field with red flow lines, the right one depicts the corresponding phase Φ_{12} revealing a V-point of index $\sigma_{12} = 6$ ($\sigma_{12} = -6$) for the shown 4-fold flower (8-fold web).

3. Tight focusing of flowers and webs

As it is known from previous work [15–28], tight focusing of polarization modulated light can reveal astonishing properties especially due to the occurence of non-negligible longitudinal z-polarization components E_z within the focal volume. In this case, RP and AP beams ($\sigma_{12} = 2$) represent the two extreme cases (see Fig. 2) containing only purely radially oriented components and no radial components at all, respectively. This means, we achieve the highest or lowest amount of z-components within the focus [15]. Beams including both, radial and azimuthal components can be realized easily by superposition of basic RP and AP modes. But in this case, the amount of both, RP and AP components, is constant within the whole transverse plane resulting in a spatially homogeneous distribution of focal z-components. In contrast, less known input light fields including a spatially structured amount of radial and azimuthal parts, will reveal spatially varying strength of focal z-polarization components, which facilitates shaping the focal volume. Vectorial flowers and webs represent these input light fields ($\vec{E^i}$, see Eq. (1)). After introducing the applied numerical method, we demonstrate the tight focusing properties of these fields, creating not yet investigated focus structures.

3.1. Numerical method

In order to calculate the focal field distribution $\vec{E}(x, y, z)$, we solve Richards and Wolf's integrals [15,31] by fast Fourier transform operations (FFT) as demonstrated in [32]. Therefore, the tailored, inhomogeneously polarized pupil function is separated into two orthogonally polarized bases, i.e. $\vec{l_0} = \left(l_{0,x}, l_{0,y}\right)$. Thus, the electric field at the exit aperture on a focal sphere (spherical coordinates (r, θ, φ)) is given by [32]

$$\vec{E^t}(\theta,\varphi) = \sqrt{\cos\theta}\left[l_{0,x}\begin{pmatrix}\cos\theta\cos^2\varphi + \sin^2\varphi\\ (\cos\theta - 1)\cos\varphi\sin\varphi\\ -\sin\theta\cos\varphi\end{pmatrix} + l_{0,y}\begin{pmatrix}(\cos\theta - 1)\cos\varphi\sin\varphi\\ \cos\theta\sin^2\varphi + \cos^2\varphi\\ -\sin\theta\sin\varphi\end{pmatrix}\right]. \tag{2}$$

Hence, focus calculations are performed for the x-polarized part of the entrance pupil (1st summand), and, independently, for the y-polarized part (2nd summand). The overall focal field is determined by the sum of the results of both calculations.

Since we apply 2D Fourier transform $\mathcal{F}$ to compute the focal distribution, which is supposed to be in real space (x, y, z), we transform the coordinates of $\vec{E^t}$ into k-space (k_x, k_y, k_z). Therefore, θ and φ are substituted according to $\cos\theta = k_z/k_0$, $\sin\theta = k_r/k_0$, $\cos\varphi = k_x/k_r$, $\sin\varphi = k_y/k_r$ with $k_z^2 = k_0^2 - k_r^2$, $k_r^2 = k_x^2 + k_y^2$ and $k_0 \sin\alpha = 1$ (α: semi aperture angle of focusing lens). Considering this, the overall focal field $\vec{E} = [E_x, E_y, E_z]^{\mathrm{T}}$ at the point (x, y, z) can be written as

$$\begin{aligned}\vec{E}(x,y,z) &= \mathcal{F}\left[\vec{E^t}(k_x,k_y)\mathrm{e}^{\mathrm{i}k_z z}k_z/k_0\right]\\ &= \mathcal{F}\left[l_{0,x}(k_x,k_y)\vec{GX}(k_x,k_y)\right] + \mathcal{F}\left[l_{0,y}(k_x,k_y)\vec{GY}(k_x,k_y)\right].\end{aligned} \tag{3}$$

Optics EXPRESS

Detailed derivation can be found in [32]. As visualized in Fig. 2(a), $\vec{GX}$ and $\vec{GY}$ include the properties of the focusing high-NA lens applied on the input light field encoded in $\vec{l}_0$. In the following we use the described approach to determine the focal field distribution $\vec{E}(x, y, 0)$ for focused vectorial flowers and spider webs $\vec{E}^i$, thus, the pupil function $\vec{l}_0$ is defined according to Eq. (1).

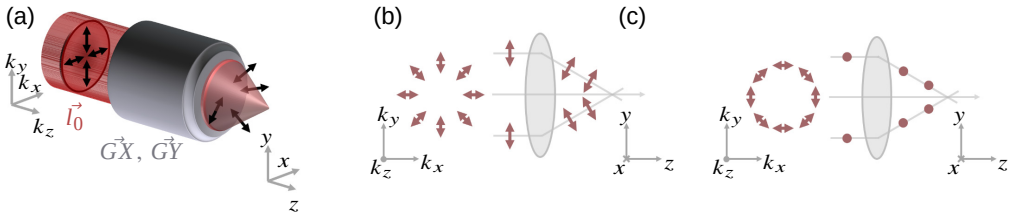

Fig. 2. Sketch of non-paraxial beam propagation of tightly focused, polarization structured light: (a) Concept image of numerical method, (b) occurence of longitudinal polarization components by focusing RP light fields, (c) focusing of AP field.

3.2. *Dark star and bright flower*

To demonstrate focal landscapes, facilitated by higher-order singular vector fields (Section 2), we exemplarily simulate the focal field distribution $\vec{E}(x, y, 0)$ of an incident light field with $\sigma_{12} = \pm 8$ resembling a 6-petal flower and a 10-fold spider web (NA = 0.9 in air, refractive index 1.0), respectively. Results are shown in Fig. 3, where (a) and (c) illustrate the incident polarization distribution by small black lines with corresponding flow lines in red and respective phase Φ_{12} of the complex Stokes field. In Φ_{12} central higher-order V-points ($\sigma_{12} = \pm 8$) are detectable. Figure 3(b) and (d) present the resulting focal intensity landscapes corresponding to (a) and (c), respectively. We show the intensity of the transverse ($|E_{x,y}|^2 \in [0, 1]$) as well as the longitudinal ($|E_z|^2 \in [0, 1]$) components next to their respective phase distributions ($\varphi_{x,y,z} \in [0, 2\pi]$). Additionally, the overall, transverse intensity distribution $|\vec{E}|^2 \in [0, 1]$ at the position of the waist of the non-paraxial beam is presented. In (b) and (d) all intensity structures are normalized individually to their maximum value, and the ratio of this maximum to the peak value of $|\vec{E}|^2$ (*peak ratio*) is given within each image (white).

For both cases, the focused flower and web, the transverse components reveal a structure of eight intensity petals, each petal showing a discrete phase value with a shift of π to its neighboring petals. Further, $|E_x|^2$ and $|E_y|^2$ are of almost equal strength. The longitudinal part $|E_z|^2$ also shows a petal structure, but consists of six (b) or ten (d) spots: The incident light fields in (a) and (c) include six and ten lines, respectively, along which the states of polarization are oriented purely radially (ζ-lines), resulting in areas of maximum value of $|E_z|^2$. Again, each intensity petal has a discrete phase value with a shift of π to adjacent petals, but shows an overall phase shift of $\pi/2$ with respect to the transverse components $\varphi_{x,y}$. This is due to differences in Gouy phase shift for x-/ y- and z-components [33]. We want to stress that, even if the peak ratio seems to be equal (b) or small (d) for the z-components in comparison to the transverse components, the spatial mean of the intensity distribution of each component shows that the z-components are about half as strong as the x-/ y-components (more details in next section). Resulting from the petal structures of individual components $|E_{x,y,z}|^2$, $|\vec{E}|^2$ represents a spatial distribution, which includes a dark star without intensity in its center (c) for the incident flower (a), or resembles a bright flower (d) for the focused spider web (b). Note that a relation between intensity landscapes and singularity index σ_{12} of the V-point of focused light field $\vec{E}^i$ can be observed, which is analysed in more detail in the following section.

Optics EXPRESS

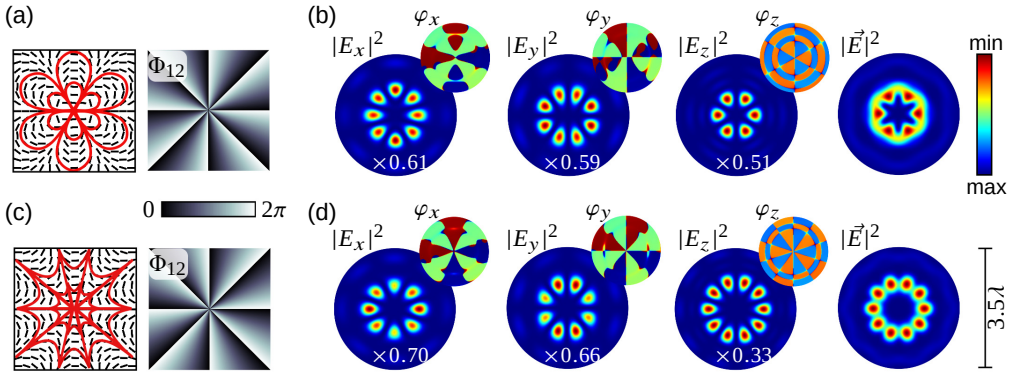

Fig. 3. Dark star and bright flower: Tight focusing (NA = 0.9) of examplary vectorial flower (a) and spider web (c) with $\sigma_{12} = \pm 8$ resulting in focal field distributions of intensity ($|E_{x,y,z}|^2$, $|\vec{E}|^2 \in [0,1]$, peak ratio within images) and phase ($\varphi_{x,y,z} \in [0, 2\pi]$) as shown in (b) and (d), respectively. The size of focal distributions is indicated by the scale bar in (d). Total intensity $|\vec{E}|^2$ resembles a dark star (bright flower) if a vectorial flower (web) is focused.

4. Tailor focal landscapes by index-to-intensity relation

Depending on the singularity index σ_{12} of higher-order V-points we are able to tailor the structure of the incident light field $\vec{E}^i$, i.e. the shape of vectorial flowers and spider webs (see Section 2). Following this, we expect a dependency between chosen singularity index of the incident field and resulting intensity structure within the focal volume. To investigate this dependency, we analyze the focal field distribution of vectorial flowers and webs of different indices, as visualized in Table 1 ($z = 0$, NA = 0.9). Table 1 shows the focal intensity landscapes for tightly focused higher-order (a) flowers, and (b) spider webs with $|\sigma_{12}| \leq 12$. The resulting normalized intensity distributions per component $|E_{x,y,z}|^2$ and overall intensity $|\vec{E}|^2$ are illustrated with respective *peak ratio* ("peak": ratio of corresponding maximum to the maximum value of $|\vec{E}|^2$) and *mean ratio* ("mean": ratio of spatial mean of $|E_{x,y,z}|^2$ to mean of $|\vec{E}|^2$).

In analogy to the examples shown in Section 3.2, the transverse components of the focal field $|E_{x,y}|^2$ for each singularity index σ_{12} reveal a petal structure, whereby the number of intensity petals is given by $|\sigma_{12}|$. Furthermore, the longitudinal parts $|E_z|^2$ resemble this distribution, but with $|\sigma_{12} - 2|$ spots, since vectorial flowers (a) and spider webs (b) include $|\sigma_{12} - 2|$ ζ-lines (see also Fig. 3 with $\sigma_{12} = \pm 8$). Thus, in this case we identify an equivalent index-to-petals relation as observed for the transverse polarization structure of vectorial flowers and webs [29], as described in Section 2. Note that the overall intensity $|\vec{E}|^2$ depicts a similar relation: Confirming the observations of Section 3.2, we observe $|\sigma_{12} - 2|$-point dark stars (a) (for $\sigma_{12} > 4$) and $|\sigma_{12} - 2|$-fold bright flowers (b).

Moreover, if the index is increased, the beam diameter increases in size, but includes a simultaneously expanding central dark area. If we take a closer look at $|E_{x,y}|^2$, this expansion in diameter and the splitting of intensity into a rising number of petals results in a general decrease of respective peak ratio. Futhermore, as indicated in Section 3.2, the mean ratio shows that $|E_z|^2$ includes about 22 % to 23 % of the total intensity $|\vec{E}|^2$, whereas transverse components $|E_{x,y}|^2$ represent about 38 % to 40 %. Since longitudinal polarization components are generated due to radially oriented parts within the incident light field, the mean ratio of $|E_z|^2$ slightly increases with the index σ_{12}, as σ_{12} defines the number of incident ζ-lines ($|\sigma_{12} - 2|$). As the consequence of increasing mean ratio of $|E_z|^2$, the according ratio of transverse components $|E_{x,y}|^2$ decreases. Thus, by the choice of σ_{12} one can tailor the amount of longitudinal and transverse components as well as the spatial structure of focal $|E_{x,y,z}|^2$-distributions and,

Optics EXPRESS

therefore, the number of points or petals of dark stars or bright flowers.

Table 1. Focal field distribution of tightly focused vectorial flowers (a) and spider webs (b) depending on index σ_{12} of singularity embedded in incident light field. Peak and mean ratio of each component $|E_{x,y,z}|^2$ is shown below respective images. Overall focal intensity distribution $|\vec{E}|^2$ resembles $|\sigma_{12}-2|$-fold stars/ flowers.

(a) Incident vectorial flower to focal dark star

σ_{12}	$\lvert E_x\rvert^2$	$\lvert E_y\rvert^2$	$\lvert E_z\rvert^2$	$\lvert\vec{E}\rvert^2$
4	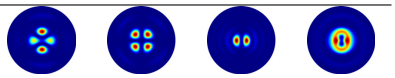			
peak	×0.76	×0.61	×0.63	
mean	×0.400	×0.378	×0.222	
6	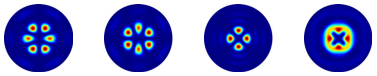			
peak	×0.62	×0.62	×0.55	
mean	×0.389	×0.389	×0.222	
8	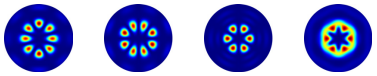			
peak	×0.61	×0.59	×0.51	
mean	×0.386	×0.387	×0.226	
10	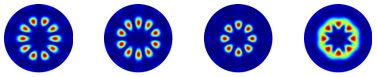			
peak	×0.56	×0.56	×0.50	
mean	×0.385	×0.385	×0.230	
12	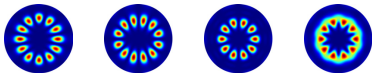			
peak	×0.56	×0.54	×0.49	
mean	×0.383	×0.384	×0.233	

(b) Incident vectorial spider web to focal bright flower

σ_{12}	$\lvert E_x\rvert^2$	$\lvert E_y\rvert^2$	$\lvert E_z\rvert^2$	$\lvert\vec{E}\rvert^2$
−4	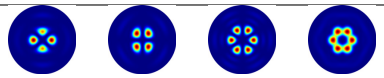			
peak	×0.75	×0.67	×0.30	
mean	×0.388	×0.390	×0.222	
−6	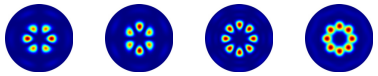			
peak	×0.72	×0.72	×0.32	
mean	×0.388	×0.388	×0.223	
−8	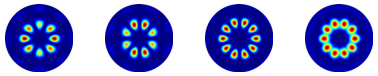			
peak	×0.70	×0.66	×0.33	
mean	×0.387	×0.388	×0.225	
−10	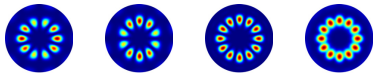			
peak	×0.68	×0.68	×0.34	
mean	×0.386	×0.386	×0.229	
−12	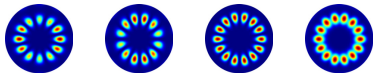			
peak	×0.67	×0.65	×0.34	
mean	×0.384	×0.384	×0.232	

5. Conclusion

We demonstrated the customization of structured, focal intensity landscapes by modulating the singularity index σ_{12} of incident vectorial flowers and spider webs. By tight focusing of these higher-order singular vector beams we are able to realize three-dimensional polarization structures $\vec{E}(x,y,z) = [E_x, E_y, E_z]^{\mathrm{T}}$ whose total intensity $|\vec{E}|^2$ resembles $|\sigma_{12}-2|$-point dark stars or $|\sigma_{12}-2|$-fold bright flowers for $z = 0$. This index-to-intensity relation is comparable to the index-to-petals or -sectors rule of incident vectorial flowers or spider webs. Moreover, each component of the focal electric field reveals a petal intensity structure, whose number of petals is given by $|\sigma_{12}|$ for $|E_{x,y}|^2$ or $|\sigma_{12}-2|$ for $|E_z|^2$. Beyond defining the shape of resulting focal field distributions, the singularity index σ_{12} also determines the strength of longitudinal polarization components in comparison to transverse ones. If the index is increased, the amount of incident RP components is enlarged, whereby the number ζ-lines is given by $|\sigma_{12}-2|$ as reflected by $|E_z|^2$-petals. Due to this increase, the mean ratio of $|E_z|^2$ raises slightly and ratio of transverse components $|E_{x,y}|^2$ decreases, without changing the NA of focusing lens. The specific shapes of realized potential landscapes as well as the ability to tailor different degrees of freedom within the focal volume by the singularity index σ_{12} will be of significant interest for a multitude of advanced applications in optical micromanipulation, material machining or high-resolution microscopy.

Optics EXPRESS

Funding

Deutsche Forschungsgemeinschaft (DFG) (EXC 1003 – CiM, TRR61).

128.176.203.23 {ts '2017-08-28 04:39:55'}